Towards retrieval of forest cover density over snow from the Multi-angle Imaging SpectroRadiometer (MISR)

Anne W. Nolin*

Department of Geosciences, Wilkinson 104, Oregon State University, Corvallis, OR 97331, USA

Abstract:

Vegetation structure and density affect the dynamics of snow accumulation and ablation. Vegetation also affects our ability to estimate snow-covered area accurately from satellite-based sensors. The objective of this case study is to demonstrate how the angular pattern of reflectance from vegetation over snow can provide information on forest cover density. Imagery from the Multi-angle Imaging SpectroRadiometer was acquired over north-central Colorado on 15 February 2002. Angular reflectance data were extracted from a variety of image locations and were analysed in conjunction with a digital elevation model and maps of forest cover density and forest cover type. The Rahman–Pinty–Verstraete semi-empirical parametric model was successfully used to simulate the angular patterns of reflectance. The model's k parameter, a measure of reflectance anisotropy, was used to characterize the angular signatures of selected pixels. Results show distinct patterns of anisotropic reflectance that depend on density and cover type. Non-forested areas exhibit a bowl-shaped pattern ($k < 1.0$) of reflectance versus viewing angle. Low-density deciduous forests also have this bowl-shaped reflectance pattern, but this changes as the density increases. Other forest cover types show transitional patterns between bowl and bell shapes and distinct bell-shaped patterns ($k > 1.0$) for higher densities. However, the relationship between k and density does not hold for forest cover densities that approach 100%. For a density of 99%, the fir–spruce forest cover type has a distinct bowl shape and a k value of only 0.69. This is in agreement with previous work indicating that sub-pixel homogeneity (whether because of sparse vegetation cover or extremely dense vegetation cover) will result in $k < 1.0$. This preliminary study indicates from a qualitative standpoint that multi-angle reflectance data captures sub-pixel-scale information on forest cover density. Copyright © 2004 John Wiley & Sons, Ltd.

KEY WORDS   MISR; snow hydrology; vegetation; angular signature; forest cover density; RPV model; Cold Land Processes Experiment

INTRODUCTION

Significance and motivation

At spatial scales ranging from 1 m to 1 km, spatio-temporal distributions of snow cover and snow water equivalent are strongly affected by vegetation density, structure, and height (Pomeroy *et al.*, 1998). Previous studies have identified the main vegetation parameters that control patterns of snow accumulation and ablation: canopy cover density and forest clearing size. Kuz'min (1960) developed a linear equation relating canopy density to accumulation for a Russian fir forest. Examining stands of aspen, pine, and spruce, Pomeroy and Goodison (1997) demonstrated a linear relationship between leaf area index and snow water equivalent. Moore and McCaughey (1997) measured a 6.4% decrease in peak snow water equivalent for every 10% increase in canopy density for a subalpine fir forest in Montana.

Snow accumulation is generally higher in forest clearings, with varying relationships between gap size and accumulation (Gary and Troendle, 1982; Gary and Watkins, 1985; Golding and Swanson, 1986; Haar 1986; Toews and Gluns, 1986; Murray and Buttle, 2003). While wind redistribution is an important factor (Pomeroy

* Correspondence to: Anne W. Nolin, Department of Geosciences, Wilkinson 104, Oregon State University, Corvallis, OR 97331, USA.
E-mail: nolina@science.oregonstate.edu

and Li, 2000; Marks *et al*., 2002), canopy interception plays a key role in snow accumulation, particularly in regions with coniferous vegetation (Pomeroy *et al*., 2002). In a study of an Oregon coniferous forest, Storck *et al*. (2002) found that up to 60% of the snow could be intercepted by the canopy. Snow ablation is influenced by vegetation, as it modifies the surface energy budget via the radiation balance and turbulent fluxes (Hardy *et al*., 1997, 1998; Koivusalo and Kokkonen, 2002). The presence of vegetation also influences optical and microwave satellite retrievals of snow-covered area (Chang *et al*., 1996; Klein *et al*., 1998), and it would be useful to have vegetation density information that could be used to correct remotely sensed snow-covered area. Thus, it is important to characterize vegetation parameters that influence the seasonal dynamics of snow accumulation and ablation and that partially conceal snow cover from satellite-based remote-sensing instruments.

Various approaches have been used in the past to estimate vegetation density in snow-dominated environments. Maps of land cover type and forest cover density exist, but they are relatively static in nature, with infrequent (>10 years) updating. Satellite-derived vegetation indices, such as the normalized difference vegetation index (NDVI; Rouse *et al*., 1974), have been widely used to map vegetation. However, the NDVI gives inaccurate results in the presence of snow, and use of NDVI from pre-snow season incorrectly characterizes the canopies of deciduous vegetation. Furthermore, NDVI is a simplistic measure of the amount of actively photosynthesizing biomass and does not provide vegetation density or canopy structure information. What is needed is a remote-sensing technique that can provide information on vegetation density and structure in the presence of snow cover.

The basis for multi-angular remote sensing: angular signatures. An 'angular signature' is the characteristic variation in reflectance as a function of viewing angle. The angular reflectance for a single pixel depends both on the intrinsic anisotropic scattering properties of the materials in the pixel and on the three-dimensional arrangement of materials. Snow is forward scattering (reflected light tends to scatter away from the source), whereas vegetation, rock and soil are backward scattering (reflected light tends to scatter back towards the source). One can begin to understand the sort of information contained in multi-angular data by considering a simple real-world example: visual observation from the window of an aircraft as one passes over a forested ridge with snow cover on the ground. The viewable fraction of snow cover is determined by the arrangement of vegetation and by the viewing angle. When the viewing angle is oblique the reflectance appears lower, since one is looking into the sides of the canopy and seeing less of the snow and more of the trees and their shadows. As the aircraft passes directly over the ridge, one is able to look directly down and see the maximum amount of snow cover for the given vegetation type and density; the reflectance is at a maximum. Further along, as one looks back at the forested ridge, the reflectance is again reduced as the viewable snow fraction decreases with increasing viewing angle. Each of the above-mentioned views has a different viewable proportion of snow and vegetation that affects the reflectance at that viewing angle. From a satellite-based sensor, variations of reflectance with viewing angle can provide details about the sub-resolution characteristics of the reflecting surface. The use of multi-angular remote sensing for characterizing surface properties represents a new paradigm in optical remote sensing. Previously, differences in anisotropic reflectance as a function of viewing angle were considered noise, not signal, and was something that needed to be corrected before the desired geophysical parameters, such as albedo or snow-covered area, could be derived. Now, rather than correcting for anisotropy, it can be exploited to gather sub-resolution information about the surface that is unique and complementary to multi-spectral information (Diner *et al*., 1999; Verstraete and Pinty, 2001).

The Multi-angle Imaging SpectroRadiometer (MISR) is an innovative instrument that uses simultaneous multi-angular measurements to obtain angular reflectance information for retrieval of geophysical parameters (Diner *et al*., 1991). MISR provides near-concurrent multiple views of a surface at several viewing geometries, with spatial resolutions of 275 m and 1·1 km (see Table I). It has excellent radiometric resolution and a wide dynamic range, preventing radiometric saturation over snow-covered surfaces, a problem with sensors such as Landsat Thematic Mapper (TM).

Table I. Description of the MISR instrument

Camera angles (camera names)	±70·5° (Df and Da); ±60·0° (Cf and Ca); ±45·6° (Bf and Ba); ±26·1° (Af and Aa); 0° (An)
Spectral bands	448 nm (blue), 558 nm (green), 672 nm (red), 866 nm (near IR)
Pixel size	275 × 275 m² (all bands in nadir camera and red bands in all other cameras) 1·1 × 1·1 km² (blue, green, and near-IR bands in fore and aft cameras)
Swath width	380 km
Quantization	14 bits, square-root encoded to 12 bits

Objectives. The primary objective of this research is to demonstrate that multi-angle reflectance data can be used to characterize some aspects of vegetation structure over snow qualitatively. Specifically, this work aims to examine: (1) whether angular patterns of anisotropic reflectance in pixels containing snow and vegetation vary depending on vegetation cover type and density; and (2) whether these angular signatures can be reproduced using a simple parametric model.

Previous work

Recent work using MISR has shown that the pattern of anisotropic reflectance from vegetation is controlled by sub-pixel-scale structure and density (Pinty *et al.*, 2002). In that investigation, the effects of vegetation canopy height and density over a bright soil substrate were examined. They used the Rahman–Pinty–Verstraete (RPV) parametric radiative transfer model (Rahman *et al.*, 1993) to simulate the shape of the reflectance function. The RPV model simulates the anisotropic behaviour of the bidirectional reflectance from a surface using a combination of three terms. The first of these is a Minneart function that describes the general shape of the angular reflectance: either increasing with viewing angle ('bowl shaped') or decreasing with viewing zenith angle ('bell shaped'). The other two terms describe the degree of forward/backward scattering and the magnitude of reflectance in the 'hot spot' direction. In the RPV model, a Minneart function parameter k is used to represent the degree of anisotropy (e.g. the degree of convexity or concavity in the bowl and bell shapes) of the reflectance function. Pinty *et al.* (2002) and Widlowski *et al.* (2001) have shown that the anisotropic reflectance pattern is controlled by vegetation structure and density at the sub-pixel scale. They found that, for a bright soil substrate with dark vegetation, the presence of medium-to-high tree densities creates a bell-shaped angular signature, whereas homogeneous vegetation (either very sparse or a closed canopy) gives a bowl-shaped pattern.

Although the k parameter is not highly descriptive of specific vegetation properties, it has been shown to be successful for limited characterization of vegetation over a bright soil. Thus, it seems appropriate to extend the use of this approach in an attempt to characterize vegetation properties over snow. The simple explanation for these two anisotropic reflectance patterns is that, when a tree canopy is underlain by bright snow, the reflectance depends heavily on the proportion of unshaded snow that is viewed by the sensor. This viewable snow fraction is a function of the vegetation type, vegetation density, and the viewing geometry. When vegetation is sparse and low growing (so shadow casting is negligible), such as in a sage–grassland setting, the reflectance is at a minimum at nadir and increases with increasing viewing angle as the snow reflectance begins to dominate at these oblique viewing angles. When trees are present, the reflectance at oblique viewing angles decreases, since the sensor is looking into the sides of the tree canopies and seeing more shadows. At a viewing angle of 0° (nadir), the viewable snow fraction is at a maximum and the effects of shadows and tree canopy are diminished, thus creating a bell-shaped angular signature. Figure 1 provides a diagrammatic representation of the effect of vegetation distribution and shadowing on angular signature. Although not shown, the case of nearly 100% vegetation density (e.g. homogeneous at the sub-pixel scale) will also lead to a bowl-shaped signature because of an increase in reflectance at oblique viewing angles in the forward and backward scattering directions.
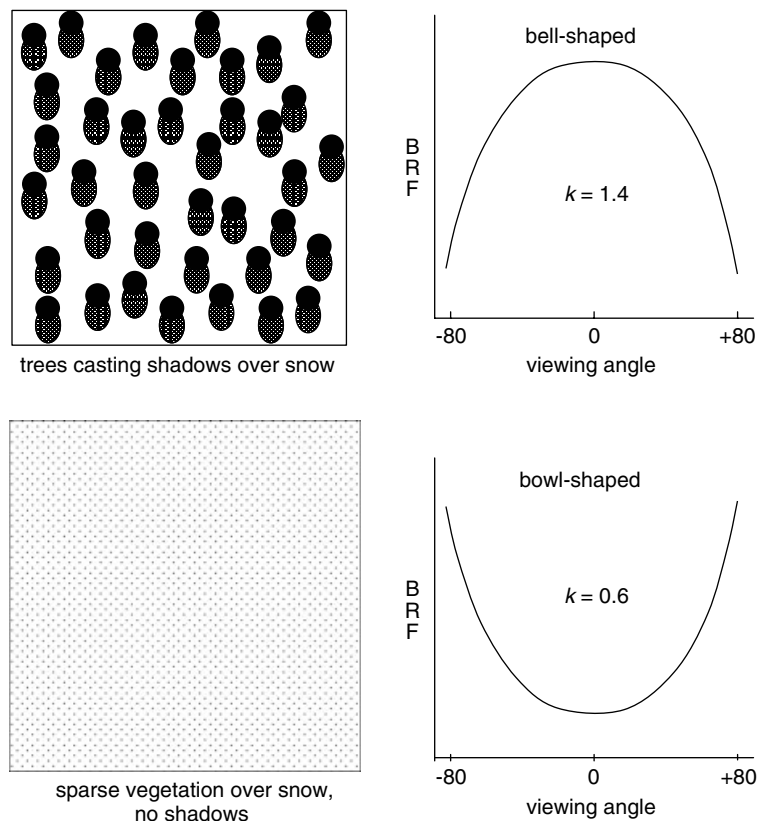
Figure 1. Diagrammatic representation of sub-pixel vegetation density and angular signatures. The left panels are a schematic representation of (top) a heterogeneous distribution of trees casting shadows over snow and (bottom) a homogeneous distribution of low, sparse vegetation over snow, where shadowing is insignificant. The sun is shining from the top of the panels (solar beam is perpendicular to the viewing azimuth). The right panels show the resulting characteristic angular signatures and representative k values

METHODOLOGY

Description of the study area

This case study focuses on a portion of the region covered in the Cold Land Processes Experiment (CLPX; http://www.nohrsc.nws.gov/~cline/clp.html). The MISR data used in this study cover the area shown in Figure 2. Data from three sub-regions are examined: North Park, Rabbit Ears, and Fraser (shown in the white rectangles in Figure 2). Each of these sub-regions differs in topography, forest cover, and snow characteristics. North Park is characterized as a sage–grassland with generally low topographic relief. Shallow drainages are present, with some larger shrubs and trees. Snow cover in this area tends to be shallow and can be patchy. The Rabbit Ears area is a higher elevation region with rolling topography. Land cover types are mixed coniferous–deciduous forests. Forest vegetation tends to form large clumps with open meadows in between. So-called 'ribbon forests' are also present in this area, in which the trees clump in long ribbon patterns perpendicular to the direction of the prevailing wind. Historical average snow water equivalent in the Rabbit Ears area for the month of February (computed using SNOTEL data from three stations for 1985–2003) is 475 mm. The Fraser area has the highest relief of the three areas. Land cover in the Fraser area is composed mostly of coniferous, subalpine forest and alpine tundra at the highest elevations. Snow in this region varies from shallow, windswept snow covers above the treeline to deeper snowpacks at lower elevations. Historical
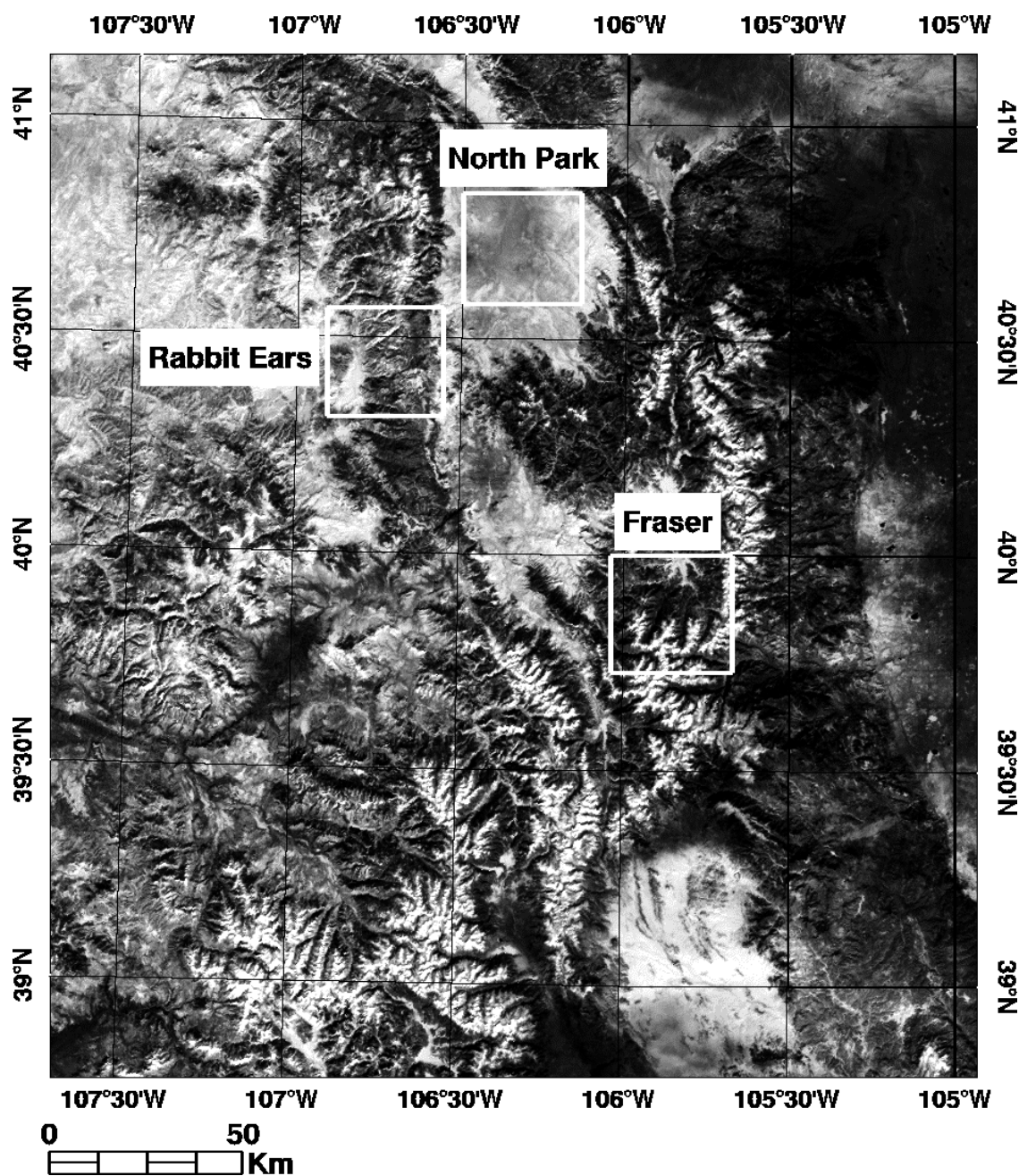
Figure 2. Map of the study area with the three sub-regions shown as the labelled white boxes. The MISR nadir camera/red channel image is shown as the base map

average snow water equivalent for the Fraser area for the month of February (computed using SNOTEL data from two stations for 1985–2003) is 277 mm.

Data description

MISR satellite imagery. MISR data were acquired on 15 February 2002. Visual inspection using composites of multiple viewing angles assured that there was no cloud cover present. Precipitation records from SNOTEL sites in the region (http://www.wcc.nrcs.usda.gov/snotel) indicate that the date of the last significant snowfall was during the period 10–11 February 2002, when the Fraser area received 0·1–0·2 in of precipitation and the Rabbit Ears area received 0·2–0·5 in of precipitation. Recorded snow water equivalent values for all five SNOTEL sites in the region exceeded 5 in at the time of the image acquisition. Therefore, it is reasonable to assume that, whereas snow cover was present on the ground, it was absent in the tree canopies.

MISR Level 1B2 (top-of-atmosphere radiometrically and geometrically calibrated radiances) data were converted to top-of-atmosphere bidirectional reflectance factors (BRFs). The BRF is defined as the ratio of upwelling radiance from a target (as measured by a detector with a specified viewing geometry) to that of a perfectly reflecting Lambertian surface. It assumes that the incident light is composed of direct beam illumination only (no diffuse illumination). The MISR BRF imagery was then geolocated, and projected into the UTM grid (WGS84 datum). To create angular signatures, only multi-angle data from the MISR red channels at 275 m spatial resolution channels were used. These include the MISR camera angles of $\pm 70 \cdot 5°$, $\pm 60°$, $\pm 45 \cdot 6°$, $\pm 25 \cdot 1°$, and nadir. Red channel data were solely used because they have the highest MISR spatial resolution; data from other channels at the oblique viewing angles are aggregated to 1·1 km. The data were recombined to create a nine-band multi-angle composite image. Solar ephemeris at the time of image acquisition was solar zenith 57·5° and solar azimuth 149° (east of north). For the central element of the MISR image, the relative azimuth between sensor and sun was 132° for the forward-viewing cameras and 48° for the aft-viewing cameras.

Ancillary data. Digital maps of forest cover type, forest cover density, and elevation were obtained from the CLPX Website and were used for land surface characterization. The forest cover type and forest cover density maps have a spatial gridding scale of 30′ and are based on Advanced Very High Resolution Radiometer (AVHRR) data (Zhu and Evans, 1994). Forest cover density represents the percentage of a grid cell that is forest covered, with values ranging from 0–100% with a cited mean accuracy of 2·02%. Grid cells with less than 25% forest cover density are classified as non-forest in the forest-cover-type map (Zhu and Evans, 1994). Classes present in the study area for this research include: fir–spruce, aspen–birch, western hardwoods, pinyon–juniper, ponderosa pine, lodgepole pine, and non-forest. Average accuracy for the forest cover types is cited as ranging from 85 to 91%, with an overall average of 89%. The digital elevation data, originally produced by the USGS, was gridded at 30 m × 30 m spacing. All the data sets were regridded to a common scale and format: 275 m scale in a UTM projection (WGS84 datum).

Method of data analysis

Angular signatures (BRF values at each of the nine MISR viewing angles) were extracted on a per-pixel basis for each forest cover type over a wide range of forest cover densities. The forest cover types had different ranges of forest cover densities. For instance, high-elevation coniferous forest cover types typically only occurred in denser configurations, whereas lower elevation forest cover types had lower densities. To reduce the effects of macroscale topography on the results, only those pixels that had slopes less than 2° were examined. Examination of over 100 pixels showed that this 2° threshold provided useful angular signatures over essentially flat surfaces while still yielding a sufficient number of pixels for examination in this study.

Albedo differences between the different selected pixels were removed by normalizing each angular signature to a zero mean and unit standard deviation. This normalization involves subtracting the mean

BRF and dividing by the standard deviation of the BRF for each set of nine BRFs that comprise an angular signature.

Using selected pixels for different forest cover types, the RPV model was run iteratively with varying k parameter until the root-mean-squared error (RMSE) of the fit of the model to the measurements was minimized. For each pixel modelled, we used the MISR-supplied values for solar zenith, solar azimuth, viewing zenith, and viewing azimuth. The solar and viewing azimuths were used to compute a relative azimuth, as is required for the RPV model.

RESULTS

MISR measurements over different forest cover types and densities

MISR angular signatures extracted for the selected pixels show a limited variety of shapes: some that are distinctly either bowl shaped or bell shaped and others that are transitional between the two. When examined by forest cover type there are distinct patterns that emerge, indicating that the shape of the angular signature depends on forest cover density and forest cover type. The pixels with particular forest cover densities were selected on the basis of two factors: (1) they described the typical range of densities for each forest cover type that were found in the region; (2) they aided in identifying the range of densities over which there is a transition between the two characteristic forms of angular signature. Although this was not always possible, in several cases the transition from bowl shaped to bell shaped (and vice versa for fir–spruce) could be demonstrated for a small range of forest cover densities.

Looking first at the deciduous forest cover type, Figure 3 shows angular signatures of western hardwoods. At 35% forest cover density, western hardwoods show a distinct bowl-shaped angular signature. There is a transition from bowl shape to bell shape that is indicated by the transitional angular signature shape for a forest cover density of 44%. At a forest cover density of 73%, the angular signature has become bell shaped.

An examination of pinyon–juniper forest cover shows a bowl shape for a forest cover density of 35% and then distinct bell shapes at 51% and 55% forest cover densities (Figure 4). No transitional pixels could be located that had sufficiently low slopes and transitional angular signatures.
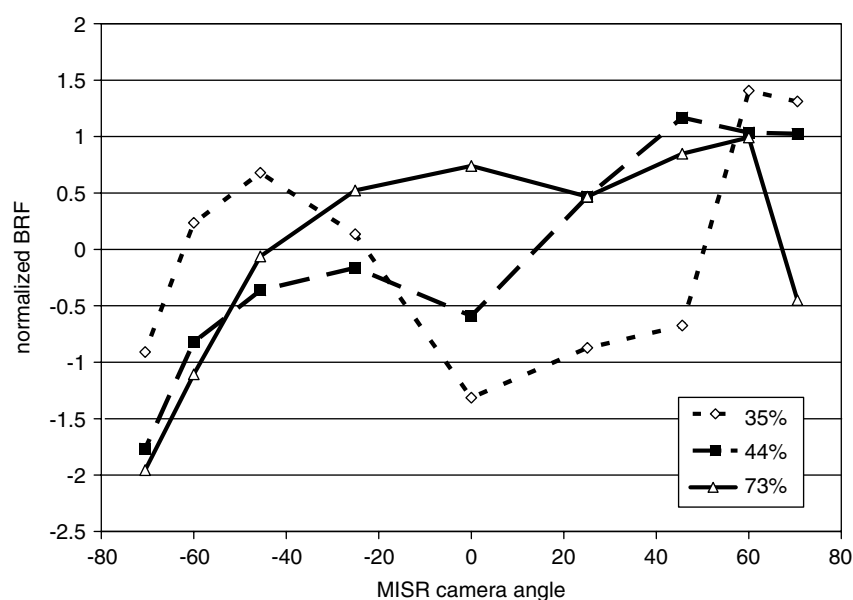

Figure 3. MISR angular signatures for three forest cover densities of western hardwoods forest
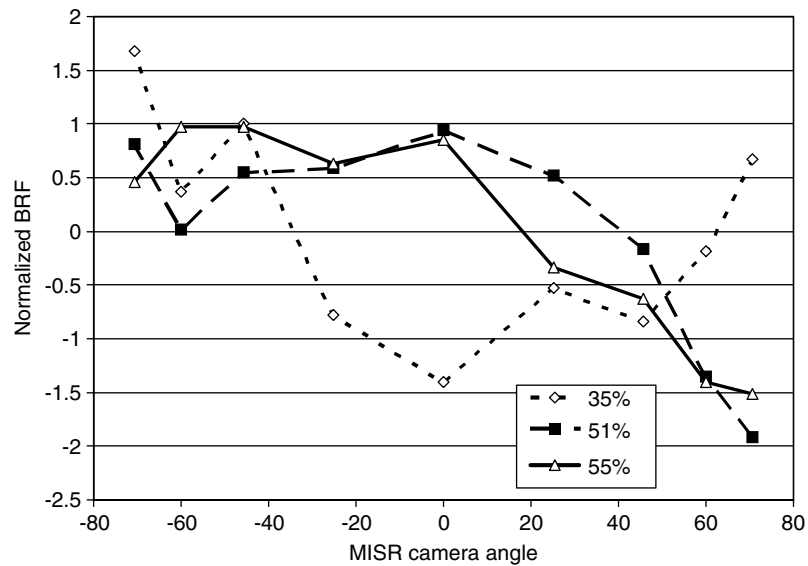
Figure 4. MISR angular signatures for three forest cover densities of pinyon–juniper forest
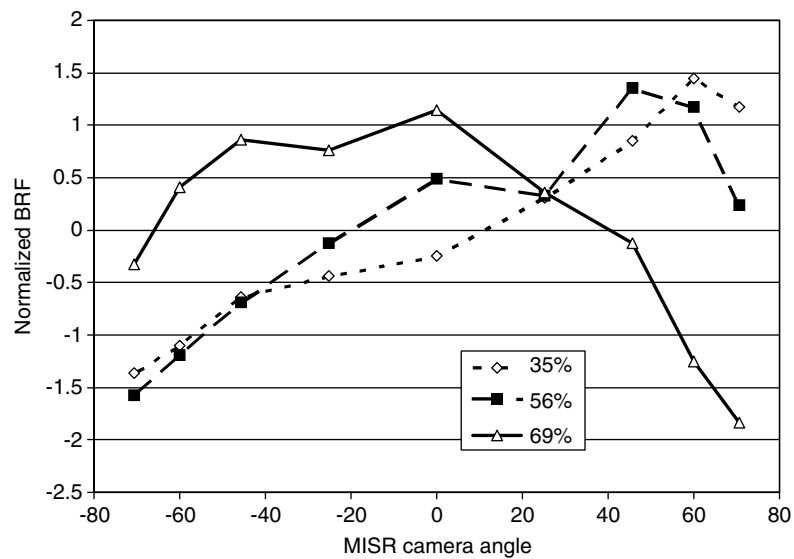

Figure 5. MISR angular signatures for three forest cover densities of ponderosa pine forest

Ponderosa pine areas do not appear to develop a bowl shape at low forest cover densities (Figure 5), but they do exhibit a transitional shape at a forest cover density of 35% (no lower densities were located in the image). At higher forest cover densities (56% and 69%) the angular signature becomes distinctly more bell shaped.

Lodgepole pine forest cover types are always bell shaped for the selected pixels (Figure 6). Low forest cover density pixels were not found in the image, probably because this forest cover type tends to have naturally higher densities. The forest cover density values are never low enough for this forest cover type to develop a bowl-shaped angular signature.
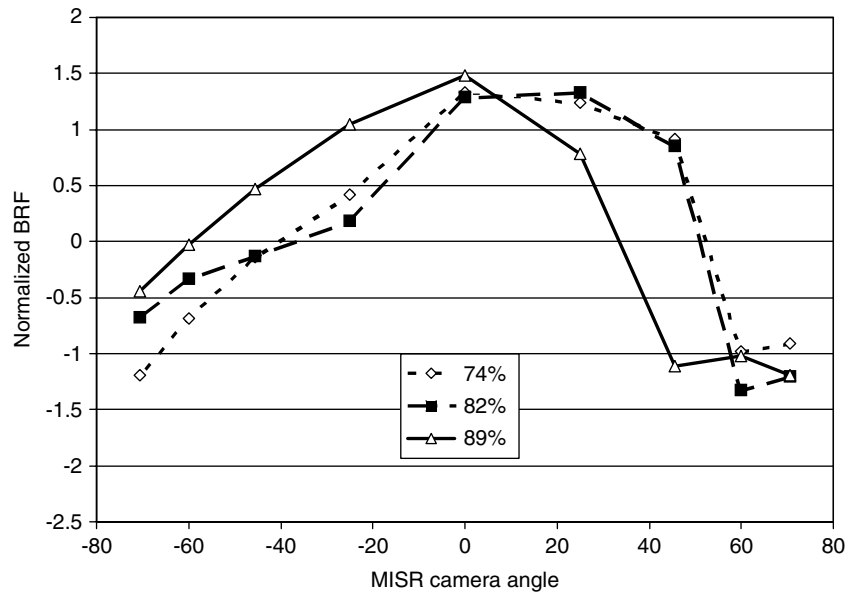
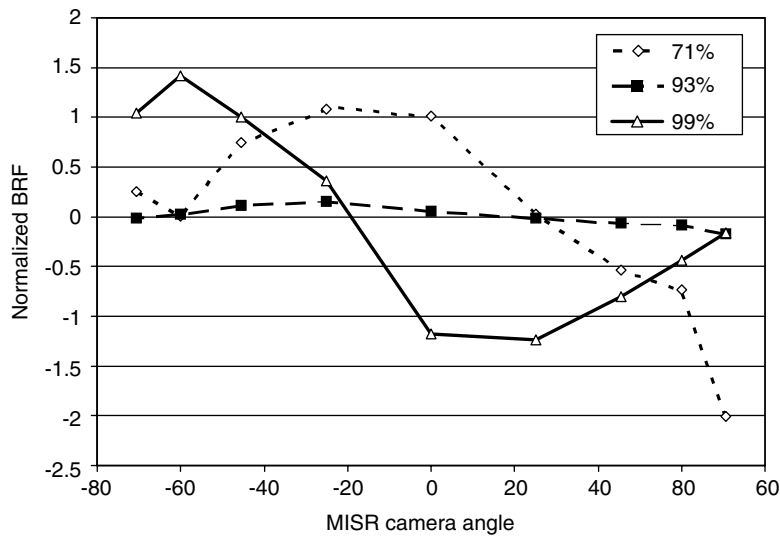Figure 6. MISR angular signatures for three forest cover densities of lodgepole pine forest

Figure 7. MISR angular signatures for three forest cover densities of fir–spruce forest

Unlike the other forest cover types, angular signatures for fir–spruce transition from bell shaped to bowl shaped as the forest cover density approaches 100% (Figure 7). As with the lodgepole pine, the fir–spruce forest cover type has high forest cover densities throughout the image. Fir–spruce exhibits the highest forest cover densities of any of the vegetation types present in the image, with numerous pixels exceeding 95% density.

The non-forested category, with densities ranging from 4 to 20%, always exhibits a bowl-shaped angular signature (Figure 8), although the patterns are not identical. This vegetation cover type is primarily found in the sage–grassland of the North Park sub-region.
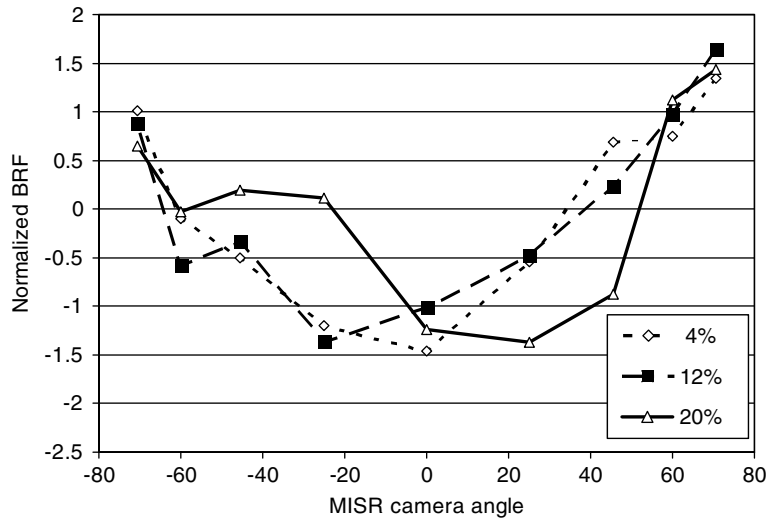
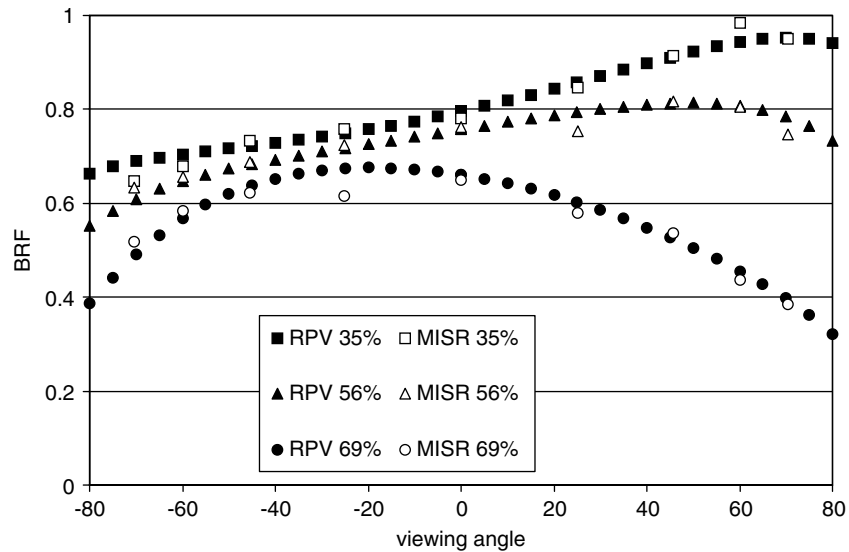Figure 8. MISR angular signatures for three cover densities of non-forested (sage–grassland) land cover

Figure 9. Measured versus modelled BRFs for three densities of ponderosa pine forest cover type (squares: 35% forest cover density; triangles: 56% forest cover density; circles: 69% forest cover density). See Table II for associated *k* values

Model results

The RPV model was able to fit effectively the MISR angular signatures for all forest cover types and densities from the selected pixels. Figures 9 and 10 show the fit of the model output to the MISR BRF values (not normalized) for ponderosa pine and fir–spruce forest cover types respectively. As these figures indicate, the model is able to simulate bowl-shaped, bell-shaped and transitional anisotropic reflectance patterns accurately. The low RMSE values reported in Table II are an indicator of the accuracy of the model fit to the data. Table II gives the values for *k* for the various forest cover types over a range of densities and the RMSE fit of the model to the MISR data. As expected, the *k* values follow the bowl-shaped, bell-shaped,
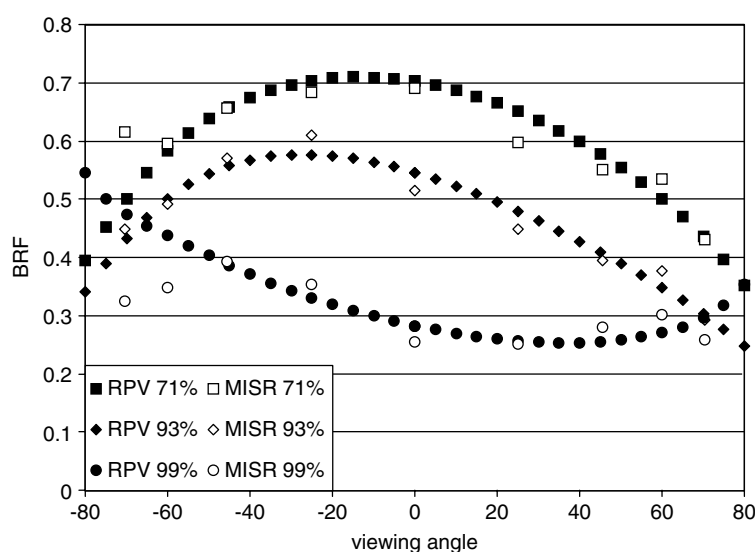
Figure 10. Measured versus modelled BRFs for three densities of fir–spruce forest cover types (squares: 71% forest cover density; triangles: 93% forest cover density; circles: 99% forest cover density). Note that the angular signature becomes strongly bowl shaped for the highest forest cover density, indicating sub-pixel homogeneity for what is likely a nearly closed canopy. See Table II for associated k values

Table II. Modeled k values and RMSE (model versus MISR BRF) for each forest cover type

Forest cover type	Forest cover density (%)	k	RMSE
Western hardwoods	35	0·90	0·000 15
	44	1·00	0·001 56
	73	1·13	0·000 01
Pinyon–juniper	35	0·99	0·000 62
	51	1·09	0·000 48
	55	1·15	0·000 57
Ponderosa pine	35	1·07	0·001 91
	56	1·14	0·001 06
	69	1·21	0·001 91
Lodgepole pine	74	1·41	0·001 23
	82	1·30	0·002 17
	89	1·36	0·000 47
Fir–spruce	71	1·20	0·001 96
	93	1·15	0·000 99
	99	0·69	0·000 19
Non-forested	04	0·89	0·000 40
	12	0·92	0·000 13
	20	0·67	0·000 46

and transitional angular signatures exhibited in Figures 3–8. It is particularly interesting to contrast the k values and angular signatures for medium-density forest cover (such as ponderosa pine, Figure 9) and for high-density forest cover (such as fir–spruce, Figure 10). At medium densities, k increases with increasing density, but k decreases at very high densities (>90%). Table II shows that at a density of 71% the k value is 1·20, declining slightly to 1·15 for a density of 93%. However, for a density of 99%, the angular signature becomes strongly bowl shaped, with a k value of only 0·69.
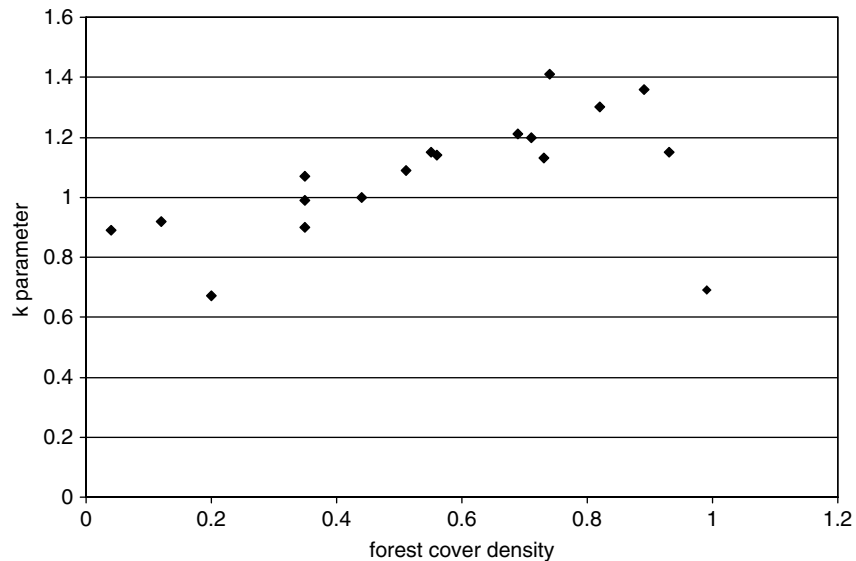
Figure 11. Modeled *k* values as a function of forest cover density for all forest cover types

This pattern is in agreement with Pinty *et al*. (2002) and Widlowski *et al*. (2001), who show that spatial homogeneity at the sub-pixel scale will result in *k* values of less than 1·0. In the case of fir–spruce forest cover type, the very dense canopy results in a homogeneous pixel producing a low *k* value. For non-forested pixels, the *k* values are also less than one, though there is a fair amount of variability between the three values, possibly indicating sub-pixel-scale topographic variability. Thus, these results appear to show that sparse vegetation and very dense forest canopy may both be considered spatially homogeneous at the sub-pixel scale.

Figure 11 plots modelled *k* values as a function of forest cover density for all selected pixels. If we exclude the *k* values for the fir–spruce forest cover type, we see a strong relationship between *k* value and forest cover type ($r^2 = 0.77$). With the fir–spruce values included, the coefficient of variation drops to 0·26. Although there are not a sufficient number of samples to produce a valid statistical result, the relationship between the *k* value and forest cover density suggests that angular signatures can provide useful sub-pixel information about forest cover density for all but the most dense forest canopies.

DISCUSSION

Qualitatively, there are clear, consistent relationships between forest cover density within each forest cover type and the pattern of multi-angle reflectance. Interpreting this in terms of the *k* parameter works as a first-order approximation. But the *k* parameter has limited physical meaning. Here, it is simply a way to categorize the shape of the anisotropic reflectance pattern. Without allometric measurements, such as tree height distributions, canopy geometry, and gap fraction, we cannot quantitatively relate the shape of the multi-angle response to vegetation parameters that are relevant to snow accumulation and ablation.

Furthermore, the 275 m spatial resolution of the MISR pixel limits the efficacy for vegetation mapping in regions where there are many smaller scale mixtures of vegetation type. The use of angular signatures as a proxy for vegetation information will not detect abrupt changes in vegetation type at the sub-pixel scale.

Atmospheric effects, although relatively minor in high-elevation regions, where optical depths are quite low, may still be considered a source of error. In a clear atmosphere, scattering will tend to make the reflected radiance slightly more isotropic. However, if undetected thin clouds are present, then these will create a

more bowl-shaped angular signature. MISR has the advantage of being able to detect optically thin clouds using multiple viewing angles, thus minimizing cloud detection errors (Di Giralomo and Wilson, 2003; Zhao and Di Giralomo, 2004). Another source of error is the mischaracterization of the ground surface. If dark rock and/or soil are exposed beneath the vegetation canopy, then this will modify the angular signature and confound interpretation. A substrate that is dark will lead to a flatter angular reflectance pattern, since the bowl-shaped/bell-shaped patterns only emerge when the substrate (snow or bright soil) is significantly brighter than the overlying vegetation. Similarly, if there were snow cover on both the canopy and the ground, then the contrast between the forest cover and the underlying surface would be reduced. The resulting angular signature would likely be a 'flatter' version of the bowl-shaped or bell-shaped angular signatures that are seen for snow-free canopies over a substrate of snowcover.

CONCLUSIONS

In summary, these preliminary results indicate that forest cover density affects angular signatures and that the RPV model does a good job of simulating the shape of anisotropic reflectance patterns over different forest cover types and densities. These qualitative results show that multi-angle remote sensing has significant potential for enhancing our characterization of vegetation in snowy environments. What remains is to be able to relate vegetation parameters quantitatively to angular signatures and potentially to use a combination of multi-spectral and multi-angle data to characterize vegetation in snow-covered pixels.

Future efforts must include physically based models, which, through inversion, will allow one to relate angular signatures to specific vegetation parameters such as the number of trees per unit area and vegetation canopy structure/geometry. Of particular interest is the GORT model (Ni *et al*., 1999), which can be inverted to estimate forest cover density and, potentially, vegetation structural parameters (Woodcock *et al*., 1997). The GORT model works well for coniferous forests on flat terrain, but in its current state problems still remain, such as corrections for topography, developing tree geometries for different forest types (including non-coniferous and non-forested), and accounting for intra-stand variance. In the future, these more physically based models should allow us to extend the modest qualitative results of this case study to provide a quantitative use of multi-angular imagery.

REFERENCES

Chang ATC, Foster JL, Hall DK. 1996. Effects of forest on the snow parameters derived from microwave measurements during the BOREAS winter field campaign. *Hydrological Processes* **10**: 1565–1574.
Di Giralomo L, Wilson M. 2003. A first look at band-differenced angular signatures for cloud detection from MISR. *IEEE Transactions on Geosciences and Remote Sensing* **41**: 1730–1734.
Diner DJ, Bruegge CJ, Martonchik JV, Bothwell GW, Danielson ED, Floyd EL, Ford VG, Hovland LE, Jones KL, White ML. 1991. A multi-angle imaging spectroradiometer for terrestrial remote sensing from the Earth Observing System. *International Journal of Imaging Systems and Technology* **3**: 92–107.
Diner DJ, Asner GP, Davies R, Knyazikhin Y, Muller J-P, Nolin AW, Pinty B, Schaaf CB, Stroeve J. 1999. New directions in earth observing: scientific applications of multiangle remote sensing. *Bulletin of the American Meteorological Society* **80**: 2209–2228.

Gary HL, Troendle CA. 1982. *Snow accumulation and melt under various stand densities in lodgepole pine in Wyoming and Colorado*. US Department of Agriculture, Forest Service, Rocky Mountain Forest and Range Experiment Station, Research Note RM-417, Government Printing Office, Washington, DC.

Gary HL, Watkins RK. 1985. Snowpack accumulation before and after thinning a dog hair stand of lodgepole pine. US Department of Agriculture, Forest Service, Rocky Mountain Forest and Range Experiment Station, Research Note RM-450, Government Printing Office, Washington, DC.

Golding DL, Swanson RH. 1986. Snow distribution patterns in clearings and adjacent forest. *Water Resources Research* **22**: 1931–1940.

Haar DR. 1986. Effects of clearcutting on rain-on-snow runoff in western Oregon: a new look at old studies. *Water Resources Research* **22**: 1095–1100.

Hardy JP, Davis RE, Jordan R, Li X, Woodcock C, Ni W, McKenzie JC. 1997. Snow ablation modeling at the stand scale in a boreal jack pine forest. *Journal of Geophysical Research, Atmospheres* **102**: 29 397–29 405.

Hardy JP, Davis RE, Jordan R, Ni W, Woodcock CE. 1998. Snow ablation modelling in a mature aspen stand of the boreal forest. *Hydrological Processes* **12**: 1763–1778.

Klein A, Hall DK, Riggs GA. 1998. Improving snow cover mapping in forests through the use of a canopy reflectance model. *Hydrological Processes* **12**: 1723–1744.

Koivusalo H, Kokkonen T. 2002. Snow processes in a forest clearing and in a coniferous forest. *Journal of Hydrology* **262**: 145–164.

Kuz'min PP. 1960. *Formirovanie Snezhnogo Pokrova I Metody Opredeleniya Snegozapasov*. Gidrometeoizdat: Leningrad. (Published 1963 as *Snow Cover and Snow Reserves*. [English Translation by Israel Program for Scientific Translation: Jerusalem]. National Science Foundation: Washington, DC).

Marks D, Winstral A, Seyfried M. 2002. Simulation of terrain and forest shelter on patterns of snow deposition, snowmelt and runoff over a semi-arid mountain catchment. *Hydrological Processes* **16**: 3605–3626.

Moore, CA, McCaughey WW. 1997. Snow accumulation under various forest stand densities at Tenderfoot Creek Experimental Forest, Montana, USA. *Proceedings of the Western Snow Conference*; 42–51.

Murray CD, Buttle JM. 2003. Impacts of clearcut harvesting on snow accumulation and melt in a northern hardwood forest. *Journal of Hydrology* **271**: 197–212.

Ni W, Li X, Woodcock CE, Caetano MR, Strahler AH. 1999. An analytical hybrid GORT model for bidirectional reflectance over discontinuous plant canopies. *IEEE Transactions on Geoscience and Remote Sensing* **37**: 987–999.

Pinty B, Widlowski J-L, Gobron N, Verstraete MM, Diner DJ. 2002. Uniqueness of multiangular measurements—part I: an indicator of subpixel surface heterogeneity from MISR. *IEEE Transactions on Geoscience and Remote Sensing* **40**: 1560–1573.

Pomeroy JW, Goodison BE. 1997. Winter and snow. In *The Surface Climates of Canada*, Bailey WG, Oke TR, Rouse WR (eds). McGill/Queen's University Press: Montreal, Quebec; 68–100.

Pomeroy JW, Li L. 2000. Prairie and arctic areal snow cover mass balance using a blowing snow model. *Journal of Geophysical Research* **105**(D21): 26 619–26 634.

Pomeroy JW, Gray DM, Shook KR, Toth B, Essery RLH, Pietroniro A, Hedstrom N. 1998. An evaluation of snow accumulation and ablation processes for land surface modelling. *Hydrological Processes* **13**: 2339–2367.

Pomeroy JW, Gray DM, Hedstrom NR, Janowicz JR. 2002. Prediction of seasonal snow accumulation in cold climate forests. *Hydrological Processes* **16**: 3543–3558.

Rahman H, Pinty B, Verstraete MM. 1993. Coupled surface–atmosphere reflectance (CSAR) model. 2. Semiempirical surface model usable with NOAA advanced very high resolution radiometer data. *Journal of Geophysical Research* **98**: 20 791–20 801.

Rouse Jr JW, Haas RH, Deering DW, Schell JA, Harlan JC. 1974. *Monitoring the vernal advancement and retrogradation (green wave effect) of natural vegetation*. NASA/GSFC Type III Final Report, Greenbelt MD.

Storck P, Lettenmaier DP, Bolton SM. 2002. Measurement of snow interception and canopy effects on snow accumulation and melt in a mountainous maritime climate, Oregon, United States. *Water Resources Research* **38**: 1–16. DOI: 10·1029/2002WR001281.

Toews DA, Gluns DR. 1986. Snow accumulation and ablation on adjacent forested and clearcut sites in southeastern British Columbia. *Proceedings of the Western Snow Conference* **54**: 101–111.

Verstraete M, Pinty B. 2002. Introduction to special section: modeling, measurement, and exploitation of anisotropy in the radiation field. *Journal of Geophysical Research* **106**: 11 903–11 907.

Widlowski J-L, Pinty B, Gobron N, Verstraete MM, Davies AB. 2001. Characterization of surface heterogeneity detected at the MISR/TERRA subpixel scale. *Geophysical Research Letters* **28**: 4639–4642.

Woodcock CE, Collins JB, Jakabhazy VD, Li X, Macomber S, Wu Y. 1997. Inversion of the Li–Strahler canopy reflectance model for mapping forest structure. *IEEE Transactions on Geoscience and Remote Sensing* **35**: 405–414.

Zhao G, Di Giralomo L. 2004. A cloud fraction vs. view angle technique for automatic in-scene evaluation of the MISR cloud mask. *Journal of Applied Meteorology* **43**: 860–869.

Zhu Z, Evans DL. 1994. U.S. forest types and predicted percent forest cover from AVHRR data. *Photogrammetric Engineering and Remote Sensing* **60**: 525–531.